BOLD activation patterns and graph metrics associated with conscious tactile perception

Short title: Brain network for tactile awareness

Martin Grund[1], Norman Forschack[1,2], Till Nierhaus[1,3], and Arno Villringer[1,4]

[1]Department of Neurology, Max Planck Institute for Human Cognitive and Brain Sciences, 04103 Leipzig, Germany

[2]Experimental Psychology and Methods, Faculty of Life Sciences, University of Leipzig, 04109 Leipzig, Germany

[3]Neurocomputation and Neuroimaging Unit, Department of Education and Psychology, Freie Universität Berlin, 14195 Berlin, Germany

[4]MindBrainBody Institute, Berlin School of Mind and Brain, Charité – Universitätsmedizin Berlin and Humboldt-Universität zu Berlin, 10099 Berlin, Germany

Corresponding author: Martin Grund, Max Planck Institute for Human Cognitive and Brain Sciences, Stephanstr. 1A, 04103 Leipzig, Germany (mgrund@cbs.mpg.de)

Number of pages: 36

Number of *figures:* 7; *tables:* 2

Number of words for *Abstract:* 175; *Introduction:* 791; *Discussion:* 1752

Conflict of interest: The authors declare no competing financial interest.

Acknowledgements: The research was funded by the Max Planck Society. We thank Ramona Menger, Anke Kummer, Mandy Jochemko, and Nicole Pampus for their data acquisition support; Bettina Johst, Hendrik Grunert, and Jöran Lepsien for their technical advice; Heike Schmidt-Duderstedt and Kerstin Flake for preparing the figures for publication; and Joshua Grant for proofreading and commenting.

Abstract

Most theories of human consciousness substantially vary in the proposed spatial extent of brain activity associated with conscious perception. Here, we investigate which local and global changes accompany conscious tactile perception. Thirty-eight healthy participants performed a tactile detection task and reported their decision confidence during fMRI. We report BOLD activations and applied graph theory to analyze the whole-brain network topologies. With confident conscious tactile perception in contrast to undetected near-threshold trials, we observed increased BOLD activity in the precuneus, the posterior cingulate cortex, the intraparietal sulcus, the insula, and the contralateral secondary somatosensory cortex. For confident misses compared to correct rejections, bilateral secondary somatosensory cortices showed greater activations. Furthermore, we assessed the whole-brain functional network topology for hits, misses and correct rejections. We did not observe any significant differences in the modularity, participation, clustering or path length of the whole-brain networks, which was supported by Bayes factor statistics. While the functional network topology did not change, conscious tactile perception emerged from greater activations at task-relevant network nodes in the posterior parietal, somatosensory and insular cortices.

Keywords

tactile perception, somatosensory processing, perceptual awareness, consciousness, functional connectivity, graph theory, fMRI

Introduction

The debate on the neural correlates of consciousness did not converge yet with regard to the spatial extent of brain activity that is necessary for conscious perception. There are particularly two opposing positions on whether the frontal or parietal cortex is the core for generating sensory experiences (Boly et al., 2017; Odegaard, Knight, & Lau, 2017). In general, there seems to be an agreement that the brain's functional network is a valuable descriptor of the underlying mechanisms of consciousness and awareness. This perspective is depicted in theories of the levels of consciousness/vigilance (Boly et al., 2011; Casali et al., 2013; King et al., 2013; Laureys, 2005; Massimini et al., 2005; Tononi, 2004; Tononi & Edelman, 1998; Tononi, Boly, Massimini, & Koch, 2016) as well as the contents of consciousness/awareness (Baars, 1988; Dehaene, Changeux, Naccache, Sackur, & Sergent, 2006; Koch, Massimini, Boly, & Tononi, 2016; Lamme, 2006; Lau & Rosenthal, 2011; Naghavi & Nyberg, 2005; Rees, Kreiman, & Koch, 2002; van Gaal & Lamme, 2012). However, the number of brain areas involved and their relationship to each other still has to be determined.

The classical approach to investigate awareness-related brain areas has been to contrast aware and unaware trials of physically identical stimuli (Aru, Bachmann, Singer, & Melloni, 2012; Baars, 1988). In the somatosensory domain, near-threshold detection paradigms performed during fMRI suggested the ipsilateral and contralateral secondary somatosensory cortices as the most promising candidates for conscious tactile perception (Moore et al., 2013; Schröder, Schmidt, & Blankenburg, 2019). Frontal and parietal activations in tactile detection paradigms have been discussed as serving the task (e.g., reporting a percept) but not the conscious sensory experience (Schröder et al., 2019). Yet, others have interpreted the fronto-parietal activity as a result of broadcasting the sensation and therefore accessing consciousness (Dehaene et al., 2006), or even being the generator for conscious

experiences by integrating sensory cortices into a posterior cortical hot zone (Koch et al., 2016). These interpretations mainly rely on the analysis of local BOLD amplitude changes, while neural interactions in task fMRI were not considered.

Another approach lies in the description of local and global changes of the functional network topology with graph theory (Bassett & Sporns, 2017). For this purpose, cortical and subcortical regions of interest (ROIs) are defined as nodes and their temporal relationships as edges (i.e., their connection; Bullmore & Bassett, 2011). The resulting network topologies are assessed with graph theory measures (e.g., modularity and clustering coefficient) and compared between experimental awareness conditions (Godwin, Barry, & Marois, 2015; Sadaghiani, Poline, Kleinschmidt, & D'Esposito, 2015; Weisz et al., 2014). *Modularity* captures the global organization of nodes in subnetworks, whereas the *clustering coefficient* indicates whether a node's neighbors are also connected with each other, thus forming local clusters. Measures of integration (e.g., *characteristic path length*) describe the general connectivity between all nodes, whereas measures of centrality (e.g., *participation coefficient*) reveal important nodes in the network. In this framework, visual awareness has recently been suggested to be accompanied by a decreased modularity and increased participation coefficient of the post-stimulus network topology in fMRI (Godwin et al., 2015). Importantly, these topologies had explanatory power beyond local BOLD amplitudes and baseline functional connectivity (Godwin et al., 2015). This indicates globally a lower segregation of nodes into distinct networks and locally a higher centrality of all nodes. A more integrated state accompanying stimulus awareness (Godwin et al., 2015) is supposed to facilitate broadcasting of sensory information to other brain areas (Dehaene et al., 2006; Dehaene & Changeux, 2011). These widespread changes in functional connectivity have been interpreted as evidence supporting global models of awareness (e.g., Global Workspace Theory; Dehaene et al., 2006; Dehaene & Changeux, 2011).

In the present study, we investigated whether the relationship between global connectivity changes and sensory awareness can be observed also for the somatosensory modality. We acquired fMRI data while participants performed a tactile detection task combined with a decision confidence rating. A special feature of the paradigm was the 9-s pause after the stimulus cue until the report to capture the post-stimulus functional connectivity free of motor movements. Furthermore, our study included 25% catch trials without electrical finger nerve stimulation. This enabled us to investigate somatosensory processing of undetected stimuli relative to correctly rejected catch trials, particularly, to test whether secondary somatosensory cortex shows a higher activation for misses compared to correct rejections. Additionally, previous studies on the association of perceptual awareness with brain functional network topologies did not investigate the topology of undetected stimuli in comparison to trials without stimulation (Godwin et al., 2015; Sadaghiani et al., 2015; Weisz et al., 2014). Hence, we provide not only the first fMRI investigation on the spatial extent of post-stimulus functional brain network alterations with conscious tactile perception but also for somatosensory processing of undetected stimuli in a near-threshold detection paradigm.

Materials & Methods

Participants

Thirty-eight healthy humans (19 women; mean age = 27.3, age range: 23-36) participated in the study. They had normal or corrected-to-normal vision and were right-handed (mean laterality index = 85, range: 60–100; (Oldfield, 1971). All participants provided informed consent (including no contra-indication for MRI) and all experimental procedures were approved by the ethics commission at the medical faculty of the University of Leipzig.

Experimental design and statistical analysis

The experimental design of the tactile detection task had the intention to generate different sensory experiences for physically identical stimulus presentations. Brain activity accompanying these sensory experiences was sampled with BOLD fMRI (see fMRI data acquisition for details). The tactile stimulation was applied as a single electrical pulse to the left index finger. The stimulation intensity was set to the individual sensory threshold, before each of the four acquisition blocks, such that participants reported a stimulus detection ("hit") in about 50% of the trials. One hundred near-threshold trials were intermingled with 20 clearly perceivable, supra-threshold trials and 40 catch trials without stimulation as control conditions. Participants had to report their perception (yes/no) and decision confidence (see "behavioral paradigm" for details). This led to three within-participant factors of interest: (a) rejected catch trials without stimulation (correct rejections), (b) non-perceived near-threshold trials (misses) and (c) perceived near-threshold trials (hits). We did not include false alarms (reported "yes" in catch trials without stimulation) due to the low false alarm rate (mean FAR = 3.3%, *SD* = 6.0%). 17 of 31 participants reported zero false alarms.

We compared the graph metrics between hits, misses and correct rejections across participants with the Wilcoxon's signed-rank test (see Graph theoretical analysis for details). For each graph metric, the *p*-values of the 24 paired Wilcoxon's signed-rank tests were corrected for multiple comparisons with a false discovery rate (FDR) of 5% (Benjamini & Hochberg, 1995). The BOLD response amplitudes were modeled for the three (detection related) within-participant factors and compared them with a mixed-effects meta-analysis (3dMEMA; Chen, Saad, Nath, Beauchamp, & Cox, 2012). We controlled for multiple comparisons with a family-wise error correction (see fMRI contrast analysis for details).

Data and code availability

The code to run the experiment, the behavioral data, and the code to analyze the behavioral and MRI data are available at http://github.com/grundm/graphCA. The structural and functional MRI data are available upon request.

Behavioral paradigm

Participants had both to report the perception (yes/no) of electrical pulses applied to their left index finger and rate their confidence about their decision. Single square-wave pulses (0.2 ms) were generated with a constant current stimulator (DS5; Digitimer) at individually assessed intensities near (mean intensity = 1.85 mA, range: 1.01-3.48 mA) and supra (mean intensity = 2.18 mA, range: 1.19-3.89 mA) perceptual threshold reflecting 50% and 100% detection rate. Additionally, 25% of all trials were catch trials without stimulation.

Each trial (21 s) started with a fixation cross (1 s), followed by a cue (1 s) indicating an electrical pulse was soon to follow (Figure 1). The stimulation onset was always 100 ms before cue offset in order to temporally align the stimulation with the detection decisions. For aware trials participants' detection decisions presumably occur the instant the stimulation is noticed. However, for unaware trials they can only conclude there was no stimulus at cue offset. If the stimulus onsets had been pseudo-randomized across the cue window, the yes decision would have occurred on average half of the cue window earlier than the no decision. The actual reporting of the decision was delayed by 9 s to allow a movement-free time window for analyses. Participants had 1.5 s to report if they felt the stimulus or not by pressing the corresponding button for yes or no. Subsequently they had another 1.5 s to report their confidence about the yes/no decision on a scale from 1 (very unconfident) to 4 (very confident). Any remaining time in the confidence rating window, following the rating, was added to a 7 s fixation cross creating an inter-trial interval of at least 7 s. Participants were instructed to place their right four fingers on a four-button box. The second and third button were controlled by the right middle finger and the ring finger to report the decision for yes or no. The outer buttons were controlled by the index finger and the little finger additionally to report the confidence decision on the full four-point scale. All button-response mappings were counterbalanced across participants. Hence depending on the mapping, the middle finger or the ring finger indicated "yes", and the four-point confidence scale started with "very confident" or "very unconfident" at the index finger.

Each block had in total 40 trials and lasted 14 min: 10 trials without stimulation, 25 with near-threshold intensity, and 5 with supra-threshold intensity, delivered in pseudo-randomized order. Before each block,

individual thresholds were assessed with an up-and-down method followed by the psi method from the Palamedes Toolbox (Kingdom & Prins, 2009). The threshold procedure followed that of the actual experimental trials but excluded the long pause and confidence response. Participants performed 4 blocks sequentially (circa 80 min). The experimental procedure was controlled by custom MATLAB scripts (MathWorks) using Psychophysics Toolbox (Kleiner et al., 2007).

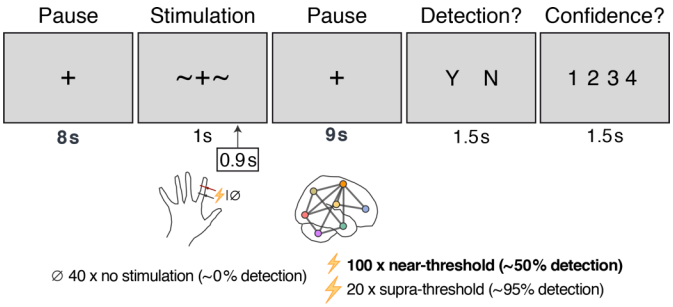

Figure 1. Experimental paradigm visualized across one trial (21 s). The tiles represent the participant's visual display and the times given below indicate the presentation duration. In total, each participant completed 160 trials across 4 blocks, including 100 near-threshold trials. Electrical nerve stimulation was applied to the left index finger 0.9 s after cue onset (~+~) to temporally align yes and no decisions, which presumably had to be made at cue offset. Participants only reported their target detection decision (yes/no) following a longer pause of 9 s in order to model the brain's post-stimulus functional network without a button press related signal. The detection decision was followed by a confidence rating on a scale from 1 (very unconfident) to 4 (very confident). Every 0.75 s a full MRI brain volume (BOLD) was acquired with a 3-mm isotropic resolution.

fMRI data acquisition

While participants performed the task, we acquired whole-brain BOLD contrast images with a 32-channel head coil on a Siemens MAGNETOM Prisma 3 Tesla scanner. For sub-second, whole-brain images (TR = 750 ms, TE = 25 ms, flip angle = 55°) we used a multiplexed echo planar imaging sequence with a multi-band acceleration factor of 3 (Feinberg et al., 2010; Moeller et al., 2010). In each of the 4 blocks we acquired 1120 brain volumes (14 min), each consisting of 36 axial slices with a field of view of 192 x 192 mm (64 x 64 voxel) and a 0.5-mm gap resulting in 3-mm isotropic voxels.

Behavioral data analysis

The behavioral data was analyzed with R 3.6.0 in RStudio 1.2.1335. Data by four participants was incomplete due to technical issues and failed data acquisition. The blocks of the remaining 34 participants were evaluated for successful near-threshold assessments if at least 4 null and 17 near-threshold trails with a yes/no and confidence response were recorded. This meant that only blocks with a hit rate at least 5% larger than the false alarm rate and participants with an average hit rate of 20-80% were further processed. This resulted in 31 participants with on average 89 near-threshold trials (range: 66-100). The distribution of mean detection rates is visualized in Figure 2a. For the confidence ratings, we calculated conditional probabilities for each confidence rating given a stimulus-response condition: correct rejection, near-threshold miss, near-threshold hit, and supra-threshold hit (Figure 2b). The conditional probabilities were compared with paired *t*-tests between neighboring conditions (correct rejection vs. near-miss, near-miss vs. near-hit, near-hit vs. supra-hit). The twelve *p*-values were FDR-corrected with a false discovery rate of 5% (Benjamini & Hochberg, 1995) and visualized with the means in Figure 2b.

fMRI preprocessing

Each EPI block was preprocessed with custom bash scripts using AFNI 18.2.17, FSL 5.0.11, and FreeSurfer 6.0.0 (http://github.com/grundm/graphCA). After removing the initial 10 volumes, the time series were despiked and corrected for slice timing. Subsequently the volumes were corrected for motion and distortion using field maps acquired in the beginning of the experiment. We applied a non-linear normalization to MNI space, before smoothing with a 7-mm FWHM kernel and scaling the time series to a mean of 100 and maximum of 200. In the final step, we calculated a nuisance regression to control for (a) motion with Friston's 24-parameter model (Friston, Williams, Howard, Frackowiak, & Turner, 1996), (b) signal outliers and their derivatives, (c) each 3 first principal components of core voxels in ventricle and white matter masks separately, and (d) trends up to polynomial of degree six (~highpass filter > 0.0046 Hz). Next to the realignment and nuisance regression of motion, we calculated the euclidean norm (enorm) to censor volumes with large motion for the functional connectivity and BOLD contrast analyses. Volumes were ignored when they exceeded motion > 0.3 mm (enorm = sqrt(sum squares) of motion parameters; AFNI 1d_tool.py -censor_motion). Compared to the framewise displacement (FD = sum(abs) of motion parameters; Power, Barnes, Snyder, Schlaggar, & Petersen, 2012), the euclidean norm has the advantage to represent appropriately large motion, e.g., the six parameters "6 0 0 0 0 0" and "1 1 1 1 1 1" would be the same for FD (FD = 6) in contrast to a enorm of 6 and

2.45, respectively. Modeling the functional connectivity and the BOLD contrasts was done with AFNI 19.1.05. All general linear models included the nuisance regressors as baseline regressors (AFNI 3dDeconvolve -ortvec).

fMRI contrast analysis

We calculated an individual general linear model (GLM) for each participant with AFNI 3dREMLfit that combined all blocks and modeled the BOLD response as a gamma function for the following conditions: correct rejections, near-threshold misses, and near-threshold hits. A second model included confident correct rejections, confident misses and confident hits. Furthermore, two BOLD response regressors for the button presses of the yes/no decision and the confidence rating were included, as well as all nuisance regressors.

The estimated regression coefficients for the aware and unaware condition were tested against each other with a mixed-effects meta-analysis (3dMEMA; Chen et al., 2012). This approach accounts for within-participant variability by using the corresponding *t*-statistics of the regression coefficients from each participant. The resulting volumes with *t*-values were corrected for multiple comparisons by thresholding voxels at $p_{voxel} < 0.0005$ and the resulting clusters at *k* voxels ($p_{cluster} = 0.05$). The cluster size threshold *k* was derived for each contrast separately based on 10,000 simulations without a built-in math model for the spatial auto-correlation function as recommended by AFNI (for details see 3dttest++ with Clustsim option and Cox, Chen, Glen, Reynolds, & Taylor, 2017) as response to (Eklund, Nichols, & Knutsson, 2016). The rendered brain images were created with MRIcron (Rorden & Brett, 2000).

Functional connectivity analysis

For estimating the context-dependent functional connectivity between regions of interest (ROI), we used the generalized psychophysiological interaction (gPPI; (McLaren, Ries, Xu, & Johnson, 2012) without the deconvolution step, as implemented in FSL (O'Reilly, Woolrich, Behrens, Smith, & Johansen-Berg, 2012). The deconvolution algorithm tries to estimate the underlying neural activity to match it temporally with the psychological context (Cisler, Bush, & Steele, 2014; Gitelman, Penny, Ashburner, & Friston, 2003; McLaren et al., 2012). However, it cannot be determined if this estimate is correct (Cole et al., 2013; O'Reilly et al., 2012). Hence, we followed the FSL implementation and convolved the psychological variable with a fixed-shaped HRF to temporally align it with the measured BOLD signal (O'Reilly et al., 2012). The gPPI model included (a) the BOLD response for each condition, (b) the baseline functional connectivity, and (c) the context-

dependent functional connectivity of a seed region of interest (ROI). For (b), the seed ROI average time series was extracted to be used as a regressor. For (c), this baseline regressor was masked for each condition separately to generate conditional interaction regressors. The mask for each condition was equivalent to the regressor that modeled the BOLD response for the corresponding condition, hence weighting the seed time series in the post-stimulus phase with the hemodynamic response. The interaction regressors for each condition allowed the estimation of (c) the context-dependent functional connectivity by accounting for (a) the BOLD response and (b) the baseline functional connectivity (Figure 5b).

The gPPI was calculated with AFNI 3dREMLfit for a whole-brain network of 264 nodes based on a resting-state functional connectivity atlas (Power et al., 2011). The nodes were defined as 4-mm radius, spherical ROIs at the atlas' MNI coordinates. The BOLD response model was a gamma function. AFNI 3dREMLfit has the advantage of allowing for serial correlations by estimating the temporal autocorrelation structure for each voxel separately.

For each node's gPPI, the coefficients of the context-dependent functional connectivity regressors were extracted from all other nodes separately by averaging across all voxels constituting the particular node. Subsequently, the beta values were combined in a symmetric connectivity matrix for each participant and each condition. As (Godwin et al., 2015) we did not assume directionality and averaged the absolute values of reciprocal connections. Subsequently, the connectivity matrices were thresholded proportionally for the strongest connections and rescaled to the range [0,1] by dividing all values by the maximum value. The figures showing nodes and edges on a glass brain (Figure 5a,e) were created with BrainNet Viewer 1.6 (Xia, Wang, & He, 2013).

Graph theoretical analysis

The context-dependent connectivity matrices were further processed with the Brain Connectivity Toolbox (BCT Version 2017-15-01; Rubinov & Sporns, 2010) to describe their network topologies. Across proportional thresholds (5-40%) graph metrics were calculated and normalized with the average graph metrics of 100 random networks with the same degree distribution (see BCT function randmio_und.m on https://sites.google.com/site/bctnet/Home/functions). In order to compare our results with the report for visual awareness (Godwin et al., 2015), we chose the same metrics for (a) segregation, (b) integration, and (c) centrality: (a) weighted undirected modularity (BCT function modulartiy_und.m; Newman, 2004) and weighted undirected clustering coefficient averaged over all nodes (BCT function clustering_coef_wu.m; Onnela,

Saramäki, Kertész, & Kaski, 2005), (b) weighted characteristic path length (BCT function charpath.m), and (c) weighted participation coefficient averaged over all nodes (BCT function participation_coef.m; Guimerà & Nunes Amaral, 2005). The participants' graph metrics were compared between each condition with the Wilcoxon's signed-rank test because the distributions of the graph metrics are unknown. The resulting 24 *p*-values for each graph metric (8 network threshold times 3 comparisons: hit vs. miss, hit vs. correct rejection, and miss vs. correct rejection) were FDR-corrected with a false discovery rate of 5% (Benjamini & Hochberg, 1995). Furthermore, we calculated the Bayes factors based on *t*-tests with a JZS prior ($r = \sqrt{2}/2$) to assess the evidence for the null hypothesis (Rouder, Morey, Speckman, & Province, 2012).

Results

Behavioral data

Participants (N = 31) detected on average 55% of the near-threshold pulses (SD = 13%), 88% of the supra-threshold pulses (SD = 12%), and correctly rejected 97% of the catch trials without stimulation (SD = 6.0%; Figure 2a). Participants reported on average to be “rather confident” or “very confident” for 87% of the correct rejections (SD = 13%), 70% of the near-threshold misses (SD = 23%), 59% of the near-threshold hits (SD = 27%) and 89% of the supra-threshold hits (SD = 13%). Participants reported significantly more often “very confident” for near-threshold misses (M = 37.2%) than hits (M = 28.7%, FDR-corrected p = 0.037) and less often “very unconfident” for misses (M = 6.9%) than hits (M = 17.7%, FDR-corrected p = 0.023; Figure 2b). The conditional probabilities for “rather unconfident” and “rather confident” did not differ between near-threshold hits and misses. Near-threshold misses and correct rejections differed in their conditional probabilities for “very unconfident”, “rather unconfident” and “very confident” (Figure 2b) indicating higher confidence for correct rejections. Also, participants were on average more confident for supra-threshold hits than near-threshold hits.

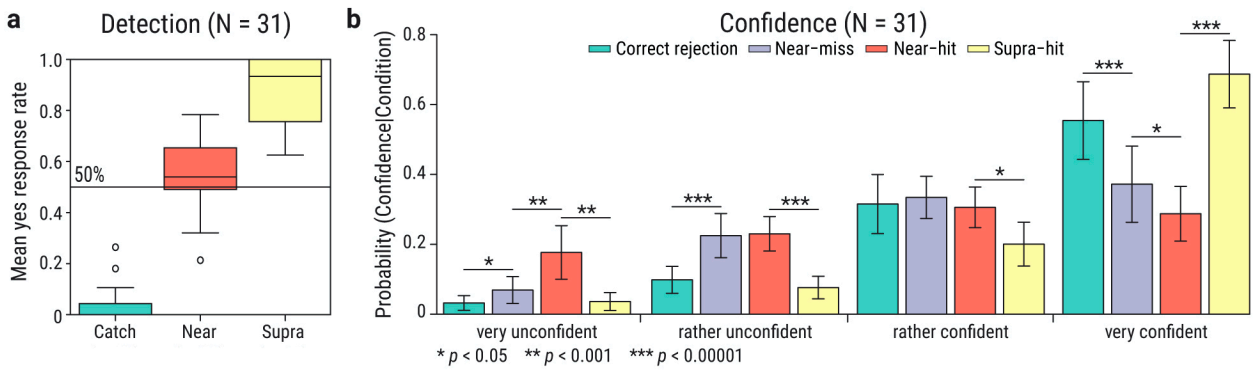

Figure 2. Mean detection rate and decision confidence across participants. (**a**) Detection rates for each trial condition: without stimulation (catch trials) and with near- and supra-threshold stimulation. The median is indicated by the central line in each box. The whiskers indicate 1.5 times the interquartile range or the maximum value if smaller. Circles indicate values beyond this whisker range. (**b**) Mean conditional probabilities for each confidence rating given a stimulus response condition: correct rejection (green), near-threshold misses (purple), near-threshold hits (red) and supra-threshold hits (yellow). Error bars indicate within-participants 95% confidence intervals (Morey, 2008). Horizontal lines indicate significant paired *t*-tests with FDR-corrected *p*-values between neighboring conditions (Benjamini & Hochberg, 1995).

BOLD amplitude contrasts

First, we modeled the BOLD contrast between hits and misses (Figure 3a-c), as well as misses and correct rejections independent of the confidence rating (Figure 3d-f). Second, we compared only confident hits and misses (Figure 4a-c), as well as confident misses and correct rejections (Figure 4d-f). For all group-level comparisons, we used the detection rate as a covariate to account for the interindividual variance (Figure 2a). Contrasting near-threshold hits and misses (stimulus awareness) showed a fronto-parietal network including the left inferior frontal gyrus (lIFG), the left nucleus accumbens (lNAC), the left and right anterior insula (lINS1; rINS), the left and right intraparietal sulcus (lIPS1; lIPS2; rIPS) and the right precuneus (rPCUN; Figure 3a-c, Table 1). When the statistical threshold for the family-wise error was set to $p_{cluster} \leq 0.06$ resulting in a decreased cluster size $k \geq 28$, two additional clusters were observed for hits compared to misses in the contralateral secondary somatosensory cortex (cS2) and the left precuneus (lPCUN). When comparing missed near-threshold trials with correctly rejected null trials (somatosensory processing of undetected stimuli), the contra- and ipsilateral S2 (cS2b; iS2), the left anterior insula (lINS2) and the left supplementary motor area (lSMA) showed statistically significant activations (Figure 3d-f).

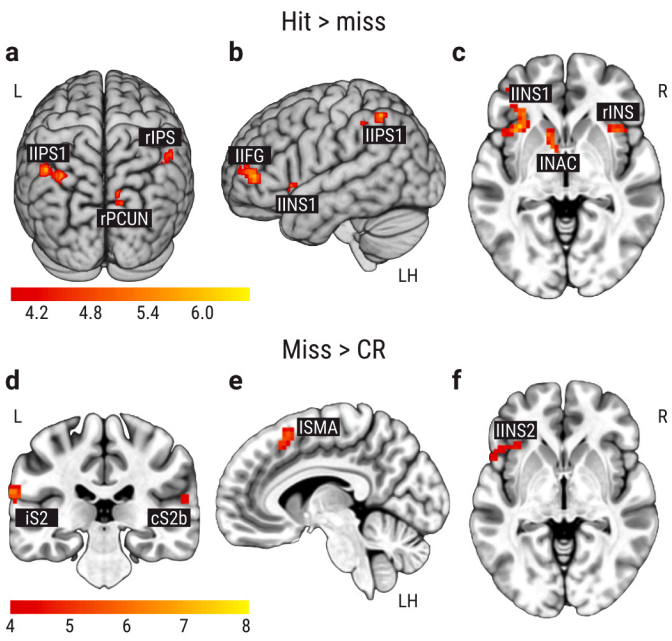

Figure 3. BOLD amplitude contrasts for awareness and stimulation effect. (**a-c**) Contrast between near-threshold hits and misses with focus on (**a**) the right precuneus (rPCUN) and the left and right intraparietal sulcus (lIPS1, rIPS1), (**b**) the left inferior frontal gyrus (lIFG) and (**c**) the left nucleus accumbens (lNAC) and the left and right anterior insula (lINS1, rINS; z = -3). Correction for multiple comparison with $t_{voxel}(30) \geq 3.92$, $p_{voxel} \leq 0.0005$ and cluster size $k \geq 31$ ($p_{cluster} \leq 0.05$). (**d-f**) Contrast between near-threshold misses and correct rejections (CR) of trials without stimulation. (**d**) Coronal view (y = -29) with the contralateral and ipsilateral secondary somatosensory cortices (cS2, iS2). (**e**) Sagittal view (x = -7) on the supplementary motor area (SMA). (**f**) Axial view (z = -3) on the left anterior insula (INS). Correction for multiple comparison with $t_{voxel}(30) \geq 3.92$, $p_{voxel} \leq 0.0005$ and cluster size $k \geq 27$ ($p_{cluster} \leq 0.05$). Left (L), right (R), and the left hemisphere (LH) are indicated.

Table 1. MNI coordinates for significant BOLD contrast clusters "hit > miss" and "miss > correct rejection (CR)" in Figure 3. Correction for multiple comparisons with $t_{voxel}(30) \geq 3.92$, $p_{voxel} \leq 0.0005$ and $p_{cluster} \leq 0.05$, resulting in a cluster size $k \geq 31$ for "hit > miss" and a cluster size $k \geq 27$ for "miss > CR". Clusters are ordered by volume (number of voxels). MNI coordinates of the maximum *t* value (peak) are reported in millimeters (mm) on the left-right (LR), posterior-anterior (PA) and inferior-superior (IS) axes. The mean *t* value is the average across all voxels of one cluster.

Contrast	Area	Label	Volume	LR	PA	IS	Mean
Hit > miss	Left anterior insula	lINS1	84	-35	19	-3	4.56
$p_{cluster} \leq 0.05$ I $k \geq 31$	Left intraparietal sulcus	lIPS1	74	-32	-62	50	4.50
$N = 31$	Right precuneus	rPCUN	64	13	-71	39	4.50
	Left nucleus accumbens	lNAC	62	-14	10	-10	4.47
	Left inferior frontal gyrus	lIFG	57	-44	46	4	4.54
	Right anterior insula	rINS	54	40	19	-7	4.56
	Right intraparietal sulcus	rIPS	42	52	-35	46	4.56
	Left intraparietal sulcus	lIPS2	37	-50	-41	46	4.21
$p_{cluster} \leq 0.06$ I $k \geq 28$	Right/contralateral S2	cS2a	30	58	-20	22	4.52
	Left precuneus	lPCUN	29	-11	-71	39	4.48
Miss > CR	Right/contralateral S2	cS2b	101	64	-20	14	4.78
$p_{cluster} \leq 0.05$ I $k \geq 27$	Left anterior insula	lINS2	75	-56	10	0	4.32
$N = 31$	Left/ipsilateral S2	iS2	52	-68	-26	22	4.73
	Left supplementary motor area	lSMA	32	-8	16	57	4.73

Second, we contrasted only confident hits, misses, and correct rejections. Trials were classified as confident when rated with 3 or 4 ("rather confident" or "very confident"). Since the first trial of each block was not considered for the fMRI analysis, the participants (N = 31) had on average 28 confident hits (SD = 14), 28 confident misses (SD = 15), and 29 confident correct rejections (SD = 7). For confident hits and misses, the precuneus bilaterally (PCUN), the left and the right intraparietal sulcus (lIPS, rIPS1, rIPS2), the posterior cingulate cortex (PCC) and the left anterior insula (lINS) had significant activation clusters with conscious tactile perception (Figure 4a-c). The contralateral secondary somatosensory cortex (cS2) showed activation again with the statistical threshold $p_{cluster} \leq 0.06$ (Table 2). Confident misses showed a higher activation than confident correct rejections in the ipsilateral and contralateral secondary somatosensory cortices (iS2, cS2). The cS2 cluster was reaching into the posterior insular cortex (Figure 4d-f).

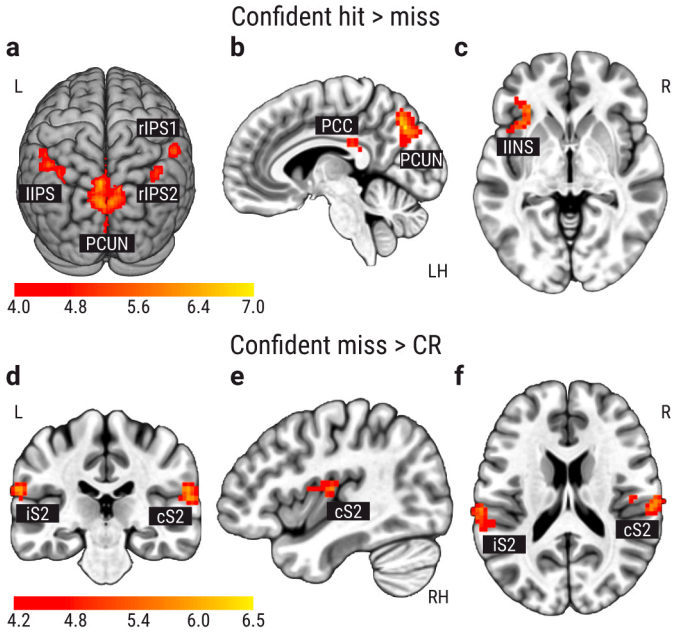

Figure 4. BOLD amplitude contrasts for only confident trials. Correction for multiple comparison with $t_{voxel}(30) \geq 3.92$, $p_{voxel} \leq 0.0005$ and cluster size $k \geq 28$ ($p_{cluster} \leq 0.05$). (**a-c**) Contrast between confident near-threshold hits and misses with focus on (**a**) the precuneus (PCUN) and the intraparietal sulcus (IPS), (**b**) the posterior cingulate cortex (PCC; x = -7), and (**c**) the left anterior insula (lINS; z = -3). (**d-f**) Contrast between near-threshold misses and correct rejections (CR) of trials without stimulation. (**d**) Coronal view (y = -26) with the contralateral and ipsilateral secondary somatosensory cortices (cS2; iS2). (**e**) Sagittal view (x = 41) on the cS2 cluster reaching into insular cortex. (**f**) Axial view on cS2 and iS2 (z = 18). Left (L), right (R), the left hemisphere (LH) and the right hemisphere (RH) are indicated.

Table 2. MNI coordinates for significant BOLD contrast clusters "confident hit > miss" and "confident miss > correct rejection (CR)" in Figure 4. Correction for multiple comparisons with $t_{voxel}(30) \geq 3.92$, $p_{voxel} \leq 0.0005$ and $p_{cluster} \leq 0.05$, resulting in a cluster size $k \geq 28$. Clusters are ordered by volume (number of voxels). MNI coordinates of the maximum *t* value (peak) are reported in millimeters (mm) on the left-right (LR), posterior-anterior (PA) and inferior-superior (IS) axes. The mean *t* value is the average across all voxels of one cluster.

Contrast	Area	Label	Volume	LR	PA	IS	Mean
Confident hit > miss	Left/right precuneus	PCUN	387	-8	-74	39	4.66
$p_{cluster} \leq 0.05$ I $k \geq 28$	Left intraparietal sulcus	lIPS	137	-47	-53	50	4.43
$N = 31$	Left anterior insula	lINS	57	-32	28	-3	4.68
	Right intraparietal sulcus	rIPS1	42	55	-38	50	4.46
	Posterior cingulate cortex	PCC	39	4	-35	22	4.45
	Right intraparietal sulcus	rIPS2	34	40	-62	53	4.33
$p_{cluster} \leq 0.06$ I $k \geq 26$	Right/contralateral S2	cS2	26	61	-20	22	4.36
Confident miss > CR	Right/contralateral S2	cS2	141	64	-20	14	4.56
$p_{cluster} \leq 0.05$ I $k \geq 28$	Left/ipsilateral S2	iS2	85	-65	-26	22	4.60

Context-Dependent Graph Measures

First, we assessed whether tactile conscious perception is accompanied by alterations of the brain's functional network topology. An atlas of 264 nodes (Power et al., 2011) was used to capture the whole-brain network as in (Godwin et al., 2015), who reported decreased modularity and increased participation with visual awareness. Whole-brain functional networks were modeled for each condition with the generalized psychophysiological interaction (gPPI; McLaren et al., 2012) without the deconvolution step (O'Reilly et al., 2012); see Methods Functional Connectivity Analysis for details). The gPPI has the advantage of controlling the context-dependent functional connectivity estimates for (a) the stimulation-related BOLD response and (b) the baseline functional connectivity across the experiment (Figure 5b). The graph theoretical analysis of the context-dependent functional connectivity matrices was performed with the Brain Connectivity Toolbox (Rubinov & Sporns, 2010) to test for changes in the same measures of integration and segregation as in (Godwin et al., 2015). We thresholded the context-dependent connectivity matrices across a range of proportional thresholds from 5% to 40% in steps of 5% (Garrison, Scheinost, Finn, Shen, & Constable, 2015) and separately calculated their normalized modularity, mean clustering coefficient, mean participation coefficient and characteristic path length (Figure 5c-f). After applying this analysis to trials independent of their confidence rating (Figure 6), we repeated the analysis for confident trials only (Figure 7) as in Godwin et al. (2015).

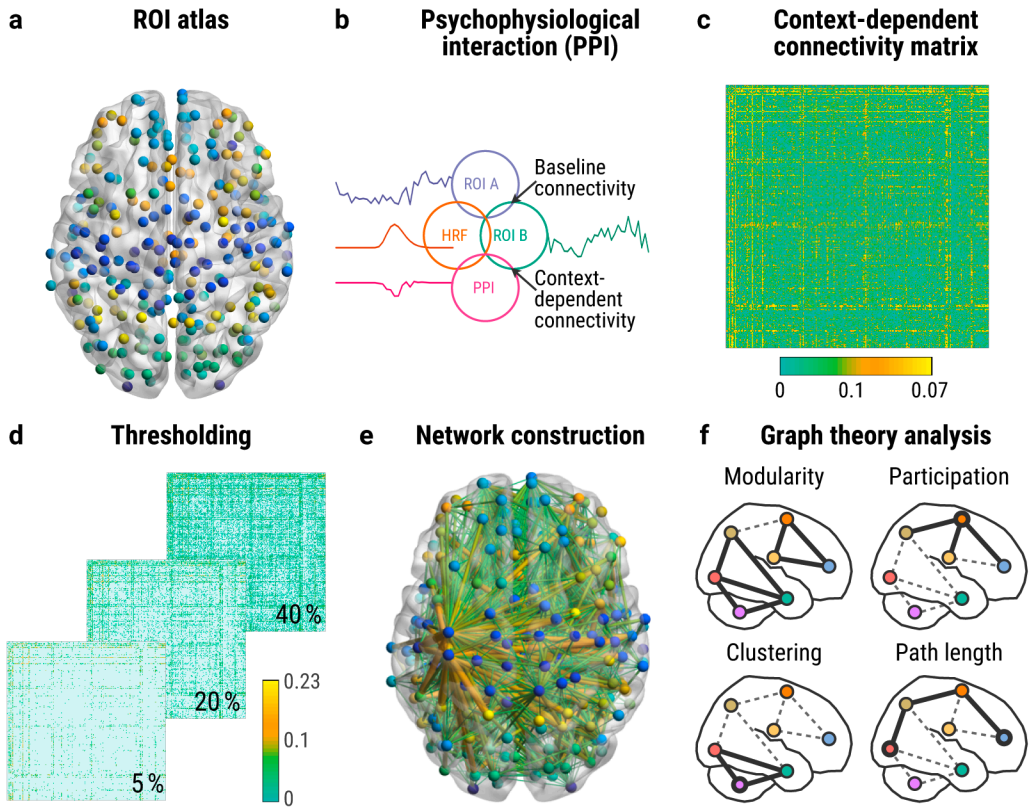

Figure 5. Context-dependent functional connectivity analysis. (**a**) Regions of interest (ROIs) were defined as 4-mm radius spheres at the MNI coordinates of an 264-nodes atlas (Power et al., 2011). (**b**) We used the generalized psychophysiological interaction (gPPI; McLaren et al., 2012) to calculate the context-dependent functional connectivity between all pairs of ROIs for each condition separately (hit, miss, and correct rejection). This measure controls for baseline functional connectivity and the stimulus-evoked hemodynamic response (HRF). (**c**) These context-dependent functional connectivity estimates were merged into individual, normalized, symmetric functional connectivity matrices to evaluate their network topology (Figure 6). For the latter, the matrices were thresholded to include only the strongest edges (**d**), and the resulting networks (**e**) were analyzed with graph theory measures (**f**). For visualization, we selected the mean context-dependent connectivity matrix for hits (**c**) and thresholded it proportionally with 5-40% (**d**) and with 5% for the visualization of the edges (**e**). Edge color and diameter capture the strength of functional connectivity. Figure concept was inspired by Figure 2 in (Uehara et al., 2014).

Hits and misses showed no significant differences in measures of global segregation into distinct networks (modularity), local segregation (clustering), integration (path length), and centrality (participation) based on paired two-sided Wilcoxon's signed-rank tests and FDR-correction (Figure 6a-d). Additionally, we calculated the Bayes factors based on paired *t*-

tests with a JZS prior ($r = \sqrt{2}/2$; Rouder et al., 2012) to evaluate the evidence for the null hypothesis (H_0: hits and misses do not differ). For modularity, participation, clustering and path length the evidence was anecdotal or moderate for the null hypothesis across the network thresholds (Figure 6e-h). Except for the 10%- and 15%-threshold, the Bayes factor for the path length was below 1 (Figure 6h) and hence reflecting anecdotal evidence for the alternative hypothesis. The path length was higher for correct rejections than hits at the 35%-threshold (FDR-corrected $p = 0.017$), and at the 40%-threshold (FDR-corrected $p = 0.042$).

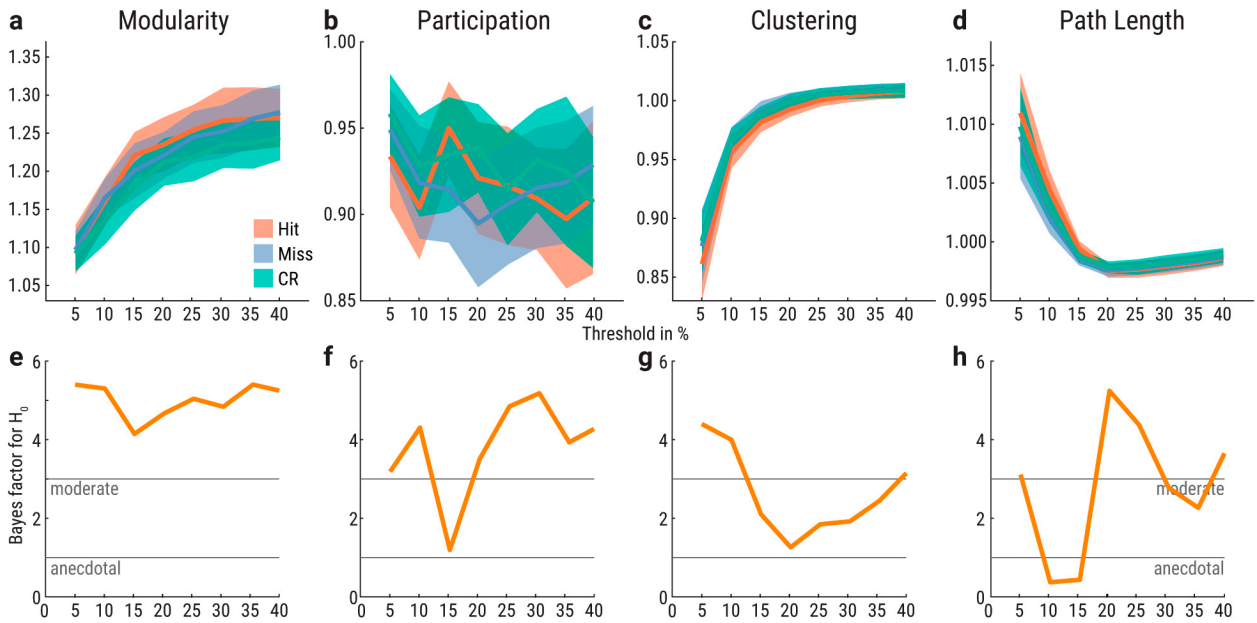

Figure 6. Functional network topology of all hits (red), misses (purple), and correct rejections (green). (**a-d**) Graph measures for network thresholds from 5-40% in 5% steps (x-axes). Y-axes indicate normalized graph metric values. Confidence bands reflect within-participant 95% confidence intervals. (**e-h**) Bayes factors (BF_{01}) based on paired *t*-test between hits and misses. Bayes factor of 2 indicates that the evidence for the null hypothesis is twice as likely compared to the alternative hypothesis given the data. Bayes factors between 1-3 are interpreted as anecdotal and between 3-10 as moderate evidence for the null hypothesis (Schönbrodt & Wagenmakers, 2018).

Since Godwin et al. (2015) analyzed the graph theoretical metrics only for confident hits and misses, we repeated the analysis for confident trials only. Trials were classified as confident

when rated with 3 or 4 (“rather confident” or “very confident”). As in the preceding analysis (Figure 6), we observed no significant differences in modularity, participation, clustering, and path length based on paired two-sided Wilcoxon’s signed-rank tests and FDR-correction (Figure 7a-d). There was anecdotal to moderate evidence for the null hypothesis (H_0: hits and misses do not differ; Fig 6e-h). Confident correct rejections showed no significant differences to confident misses or confident hits (Figure 7a-d).

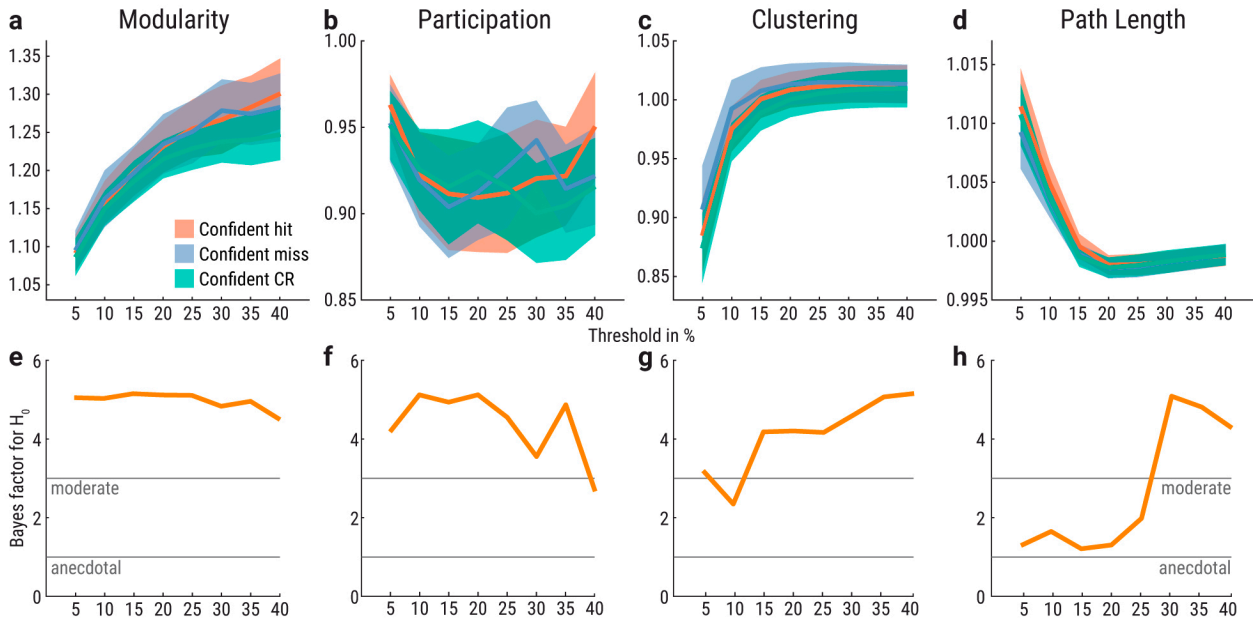

Figure 7. Functional network topology of only confident hits (red), misses (purple), and correct rejections (green). (**a-d**) Graph measures for network thresholds from 5-40% in 5% steps (x-axes). Y-axes indicate normalized graph metric values. Confidence bands reflect within-participant 95% confidence intervals. (**e-h**) Bayes factors (BF_{01}) based on paired *t*-tests between confident detected and undetected near-threshold trials. Bayes factor of 2 indicates that the evidence for the null hypothesis is twice as likely compared to the alternative hypothesis given the data. Bayes factors between 1-3 are interpreted as anecdotal and between 3-10 as moderate evidence for the null hypothesis (Schönbrodt & Wagenmakers, 2018).

Discussion

Using fMRI during a near-threshold somatosensory detection task, we addressed the question of whether conscious perception is accompanied by local brain activity and functional brain network topology alterations. The spatial extent of such (presumed) alterations, whether localized within a specific perceptual modality or global, has important implications for awareness theories. With confident conscious tactile perception in comparison to undetected stimuli, we observed a higher activation in the posterior parietal and insular cortices. In contrast to the reported breakdown of the whole-brain modularity with visual awareness (Godwin et al., 2015), our graph-theoretical analysis of the network topology could not provide evidence for a difference between aware and unaware trials in modularity, participation, clustering, or path length. Furthermore, we also did not observe stimulation-related functional network alterations for detected or undetected near-threshold trials compared to trials without stimulation.

When contrasting the stimulus-evoked BOLD responses for hits and misses, the left and right anterior insula, the left and right intraparietal sulcus, the right precuneus, the left inferior frontal gyrus, and the left nucleus accumbens showed higher activation for conscious perception (Table 1). The contrast for only confident hits and misses showed a similar pattern with the left anterior insula, the left and right intraparietal sulcus, the bilateral posterior cingulate cortices, and the bilateral precuneus (Table 2), but excluding significant clusters in the left inferior frontal gyrus, the left nucleus accumbens, and the right anterior insula. This might be due to the absent decision confidence difference because the ventral striatum (entailing the nucleus accumbens) has been reported to encode confidence in a visual motion discrimination task (Hebart, Schriever, Donner, & Haynes, 2016). Also, the anterior insula correlated with uncertainty in a tactile detection task (Schröder, Schmidt, & Blankenburg, 2019). Based on a no-report binocular rivalry paradigm, it has been argued

that frontal activity relates to introspection and action but not to perception (Frässle, Sommer, Jansen, Naber, & Einhäuser, 2014). This might also explain why the inferior frontal gyrus is not anymore among the significant clusters when we controlled for confidence. In contrast to the absence of posterior parietal activity in a task that orthogonalized the report from the perception and required an immediate response (Schröder, Schmidt, & Blankenburg, 2019), we found a prominent activation in the precuneus and the posterior cingulate cortex for hits compared to misses. One possible explanation is that our task had a 9-s pause after the stimulation until the report to capture the context-dependent functional connectivity and hence required more working memory capacities. Recent literature has argued the default mode network (e.g., posterior cingulate cortex) supports a stronger global workspace configuration that improves working memory performance (Vatansever et al., 2015) and might be beneficial for conscious perception. Based on a literature review of the neural correlates of consciousness and new no-report paradigms (Frässle, Sommer, Jansen, Naber, & Einhäuser, 2014), others have highlighted the role of the posterior cortex as a “hot zone” for conscious sensory experiences (Koch et al., 2016).

Next to the somatosensory and insular cortices, the inferior and superior parietal lobe, and the supplementary and cingulate motor areas have been reported for somatosensory processing (Ruben et al., 2001). When Godwin et al. (2015) compared the BOLD responses between confident aware and unaware trials for visual stimulation, they observed a more circumscribed positive activity pattern than the global changes in connectivity. They reported clusters in the left ventro-lateral prefrontal cortex (VLPFC), the pre-supplementary motor area (PreSMA), the left middle frontal gyrus (MFG), the bilateral inferior parietal lobule (IPL), and the left intraparietal sulcus (IPS). This pattern, similar to our findings, is also missing the primary sensory areas. Yet, this fronto-parietal network was not driving the decreased

modularity and increased participation. Both topology effects were also present in a network that excluded the eight nodes overlapping with the activation sites (Godwin et al., 2015).

In the current study, the contralateral secondary somatosensory cortex (cS2) was found for both contrasts “hit > miss” and “confident hit > miss” when the statistical cluster threshold was set to $p = 0.06$. This is interesting in the context of the debate, which role cS2 has for conscious somatosensory perception. An fMRI study on vibrotactile detection reported ipsilateral and contralateral S2 as the best correlate for detection success (Moore et al., 2013). In stroke patients, we have previously shown that - despite intact S1 - also lesions in S2 (along with anterior and posterior insula, putamen, and subcortical white matter connections to prefrontal structures) lead to impaired tactile conscious experience (Preusser et al., 2015). In an EEG study, the detection of near-threshold electrical pulses to the finger was best explained by the recurrent processing between contralateral S1 and S2, as well as contralateral and ipsilateral S2 (Auksztulewicz, Spitzer, & Blankenburg, 2012). Recently, it has been claimed that bilateral S2 is the locus of conscious tactile perception because its BOLD activity across a range of ten electrical near-threshold intensities (0-100% hit rate) was best explained by a psychometric function (Schröder et al., 2019). However, our study allowed also to contrast misses and correct rejections - i.e., revealing stimulus-locked activations despite negative behavioral responses - resulting in a higher activation in the left anterior insula, the left supplementary area, and the bilateral S2 for missed near-threshold trials (Table 1). Next to trials without stimulation, our study had additionally the advantage to previous tactile detection fMRI studies (Moore et al., 2013; Schröder et al., 2019) that it allowed to control for the decision confidence. For the contrast of only confident misses and correct rejections, there was a higher activation only in the ipsilateral and contralateral S2, reaching into right posterior insula (Figure 4, Table 2). Hence, despite participants reported with confidence in misses and correct rejections that they did not perceive a stimulus, we

observed the activation sites in the somatosensory and insular cortices expected for somatosensory perception (Blankenburg et al., 2003; Pleger & Villringer, 2013; Ruben et al., 2001). One possible explanation is that activity in the contralateral secondary somatosensory cortex has to reach first a specific threshold for conscious tactile perception. This can happen due to recurrent processing between contralateral S1 and S2, and bilateral S2 which amplifies the activity in cS2 (Auksztulewicz, Spitzer, & Blankenburg, 2012). Furthermore, the secondary somatosensory cortex might serve multiple functions. Next to the correlation of most voxels in cS2 with a psychometric function, it has been reported that more inferior and superior parts of cS2 correlated with a binary detection function, and more posterior and anterior parts of cS2 correlated with a linear intensity function (Schröder et al., 2019). In our study, the cS2 cluster for the contrast "miss > correct rejection" was more inferior (y = 64; y = -20, z = 14) than the cS2 cluster for the contrast "hit > miss" (x = 58, y = -20, z = 22; Table 1). The same z-coordinates were observed for only confident trials (Table 2). Thus, the cS2 cluster for conscious perception in our study was closest to the cS2 cluster associated with detection probability (R SII: x = 56, y = -16, z = 20), and the cS2 cluster for undetected near-threshold stimuli was closest to the inferior cS2 cluster associated with detection (R SIIi: x = 52, y = -22, z = 8; Schröder et al., 2019). For the latter, we would have predicted the closest distance to the cS2 cluster associated with intensity (R SIIp: x = 62, y = -34, z = 22; R SIIa: x = 54, y = -6; z = 4; Schröder et al., 2019) because there is no difference regarding "detection" for misses compared to correct rejections.

Furthermore, the SMA was reported to explain the activity of the report best and the anterior insula to correlate with uncertainty (Schröder et al., 2019). Both clusters were present in the contrast of misses and correct rejections (Table 1) but not in the contrast of only confident misses and correct rejections (Table 2). Also, in the comparison of hits and misses, the left and right anterior insula showed significant activations (Table 1). However,

when we compared only confident hits and misses, the left anterior insula was still significant (Table 2). One reason might be the reported option “very confident” was significantly more frequent for misses than hits, while there was no difference for “rather confident” between hits and misses (Figure 2b). That is why a higher activation of the anterior insula for confident hits than misses could be a correlate of the higher uncertainty in confident hits (less frequent “very confident”).

While controlling for stimulus-evoked BOLD responses and baseline functional connectivity, we did not observe context-dependent functional connectivity changes that result in network topology alterations through modularity, participation, clustering and path length between hits and misses. The isolated network topology differences between correct rejections and hits at the 35-40%-threshold for path length (Figure 6d) were not consistent across thresholds and not present in the analysis of only confident trials. That is why we do not interpret these differences as a valid and reliable effect. Thus, there was neither a functional network alteration by stimulus awareness (hit > miss) nor by the detected (hit > CR) or undetected stimulation (miss > CR).

One reason why Godwin et al. (2015) observed whole-brain network topology alterations for visual awareness might be the missing physical similarity between aware and unaware trials. Hits and misses originated from two different masking conditions: backward masking generated 83% of all hits and forward masking 84% of all misses. Additionally, their total number of trials for 24 participants was not balanced (276 confident misses vs. 486 confident hits). In contrast, our study did not rely on masking the target stimulus and resulted in a balanced total amount of 882 confident misses and 870 confident hits for 31 participants (Figure 7). Furthermore, we also present the results of 1507 hits, and 1190 misses independent of the confidence rating (Figure 6). Future studies investigating visual awareness may be able to distill conscious percepts for present stimuli without confounding

masking conditions, for instance taking advantage of sub-millisecond precision of modern tachistoscopes (Sperdin, Repnow, Herzog, & Landis, 2013).

In summary, our well controlled paradigm shows that while the whole-brain functional connectivity does not change, task-relevant network nodes decide whether a weak electrical pulse enters consciousness or not. In contrast to previously reported global changes, the spatial extent of the observed amplitude alterations in the posterior parietal, somatosensory and insular cortices with conscious tactile perception is very circumscribed. Each region might contribute a specific component to the overall conscious percept.

References

Aru, J., Bachmann, T., Singer, W., & Melloni, L. (2012). Distilling the neural correlates of consciousness. *Neuroscience and Biobehavioral Reviews*, *36*(2), 737–746. http://doi.org/10.1016/j.neubiorev.2011.12.003

Auksztulewicz, R., Spitzer, B., & Blankenburg, F. (2012). Recurrent neural processing and somatosensory awareness. *Journal of Neuroscience*, *32*(3), 799–805. http://doi.org/10.1523/JNEUROSCI.3974-11.2012

Baars, B. J. (1988). A cognitive theory of consciousness. Cambridge [England] ; New York : Cambridge University Press.

Bassett, D. S., & Sporns, O. (2017). Network neuroscience. *Nature Neuroscience*, *20*(3), 353–364. http://doi.org/10.1038/nn.4502

Benjamini, Y., & Hochberg, Y. (1995). Controlling the False Discovery Rate: A Practical and Powerful Approach to Multiple Testing. *Royal Statistical Society, Series B Methodological*, *57*(1), 289–300. http://doi.org/10.2307/2346101

Blankenburg, F., Taskin, B., Ruben, J., Moosmann, M., Ritter, P., Curio, G., & Villringer, A. (2003). Imperceptible stimuli and sensory processing impediment. *Science*, *299*(5614), 1864–1864. http://doi.org/10.1126/science.1080806

Boly, M., Garrido, M. I., Gosseries, O., Bruno, M.-A., Boveroux, P., Schnakers, C., et al. (2011). Preserved feedforward but impaired top-down processes in the vegetative state. *Science*, *332*(6031), 858–862. http://doi.org/10.1126/science.1202043

Boly, M., Massimini, M., Tsuchiya, N., Postle, B. R., Koch, C., & Tononi, G. (2017). Are the Neural Correlates of Consciousness in the Front or in the Back of the Cerebral Cortex? Clinical and Neuroimaging Evidence. *Journal of Neuroscience*, *37*(40), 9603–9613. http://doi.org/10.1523/JNEUROSCI.3218-16.2017

Bullmore, E. T., & Bassett, D. S. (2011). Brain graphs: graphical models of the human brain connectome. *Annual Review of Clinical Psychology*, *7*, 113–140. http://doi.org/10.1146/annurev-clinpsy-040510-143934

Casali, A. G., Gosseries, O., Rosanova, M., Boly, M., Sarasso, S., Casali, K. R., et al. (2013). A Theoretically Based Index of Consciousness Independent of Sensory Processing and Behavior. *Science Translational Medicine*, *5*(198), 198ra105–198ra105. http://doi.org/10.1126/scitranslmed.3006294

Chen, G., Saad, Z. S., Nath, A. R., Beauchamp, M. S., & Cox, R. W. (2012). FMRI group analysis combining effect estimates and their variances. *NeuroImage*, *60*(1), 747–765. http://doi.org/10.1016/j.neuroimage.2011.12.060

Cisler, J. M., Bush, K., & Steele, J. S. (2014). A comparison of statistical methods for detecting context-modulated functional connectivity in fMRI. *NeuroImage*, *84*, 1042–1052. http://doi.org/10.1016/j.neuroimage.2013.09.018

Cole, M. W., Reynolds, J. R., Power, J. D., Repovs, G., Anticevic, A., & Braver, T. S. (2013). Multi-task connectivity reveals flexible hubs for adaptive task control. *Nature Neuroscience*, *16*(9), 1348–1355. http://doi.org/10.1038/nn.3470

Cox, R. W., Chen, G., Glen, D. R., Reynolds, R. C., & Taylor, P. A. (2017). FMRI Clustering in AFNI: False-Positive Rates Redux. *Brain Connectivity*, *7*(3), 152–171. http://doi.org/10.1089/brain.2016.0475

Dehaene, S., & Changeux, J.-P. (2011). Experimental and theoretical approaches to conscious processing. *Neuron*, *70*(2), 200–227. http://doi.org/10.1016/j.neuron.2011.03.018

Dehaene, S., Changeux, J.-P., Naccache, L., Sackur, J., & Sergent, C. (2006). Conscious, preconscious, and subliminal processing: a testable taxonomy. *Trends in Cognitive Sciences*, *10*(5), 204–211. http://doi.org/10.1016/j.tics.2006.03.007

Eklund, A., Nichols, T. E., & Knutsson, H. (2016). Cluster failure: Why fMRI inferences for spatial extent have inflated false-positive rates. *Proceedings of the National Academy of Sciences of the United States of America*, *113*(28), 7900–7905. http://doi.org/10.1073/pnas.1602413113

Feinberg, D. A., Moeller, S., Smith, S. M., Auerbach, E., Ramanna, S., Gunther, M., et al. (2010). Multiplexed echo planar imaging for sub-second whole brain FMRI and fast diffusion imaging. *PLoS ONE*, *5*(12), e15710. http://doi.org/10.1371/journal.pone.0015710

Frässle, S., Sommer, J., Jansen, A., Naber, M., & Einhäuser, W. (2014). Binocular rivalry: frontal activity relates to introspection and action but not to perception. *Journal of Neuroscience*, *34*(5), 1738–1747. http://doi.org/10.1523/JNEUROSCI.4403-13.2014

Friston, K. J., Williams, S., Howard, R., Frackowiak, R. S., & Turner, R. (1996). Movement-related effects in fMRI time-series. *Magnetic Resonance in Medicine*, *35*(3), 346–355.

Garrison, K. A., Scheinost, D., Finn, E. S., Shen, X., & Constable, R. T. (2015). The (in)stability of functional brain network measures across thresholds. *NeuroImage*, *118*, 651–661. http://doi.org/10.1016/j.neuroimage.2015.05.046

Gitelman, D. R., Penny, W. D., Ashburner, J., & Friston, K. J. (2003). Modeling regional and psychophysiologic interactions in fMRI: the importance of hemodynamic deconvolution. *NeuroImage*, *19*(1), 200–207. http://doi.org/10.1016/S1053-8119(03)00058-2

Godwin, D., Barry, R. L., & Marois, R. (2015). Breakdown of the brain's functional network modularity with awareness. *Proceedings of the National Academy of Sciences of the United States of America*, *112*(12), 3799–3804. http://doi.org/10.1073/pnas.1414466112

Guimerà, R., & Nunes Amaral, L. A. (2005). Functional cartography of complex metabolic networks. *Nature*, *433*(7028), 895–900. http://doi.org/10.1038/nature03288

Hebart, M. N., Schriever, Y., Donner, T. H., & Haynes, J.-D. (2016). The Relationship between Perceptual Decision Variables and Confidence in the Human Brain. *Cerebral Cortex*, *26*(1), 118–130. http://doi.org/10.1093/cercor/bhu181

King, J.-R., Sitt, J. D., Faugeras, F., Rohaut, B., Karoui, El, I., Cohen, L., et al. (2013). Information sharing in the brain indexes consciousness in noncommunicative patients. *Current Biology*, *23*(19), 1914–1919. http://doi.org/10.1016/j.cub.2013.07.075

Kingdom, F. A. A., & Prins, N. (2009). Psychophysics (pp. 1–297). London: Academic Press Inc.

Kleiner, M., Brainard, D., Pelli, D., Ingling, A., Murray, R., & Broussard, C. (2007). What's new in psychtoolbox-3. *Perception*, *36*(14), 1–16.

Koch, C., Massimini, M., Boly, M., & Tononi, G. (2016). Neural correlates of consciousness: progress and problems. *Nature Reviews Neuroscience*, *17*(5), 307–321. http://doi.org/10.1038/nrn.2016.22

Lamme, V. A. F. (2006). Towards a true neural stance on consciousness. *Trends in Cognitive Sciences*, *10*(11), 494–501. http://doi.org/10.1016/j.tics.2006.09.001

Lau, H., & Rosenthal, D. (2011). Empirical support for higher-order theories of conscious awareness. *Trends in Cognitive Sciences*, *15*(8), 365–373. http://doi.org/10.1016/j.tics.2011.05.009

Laureys, S. (2005). The neural correlate of (un)awareness: lessons from the vegetative state. *Trends in Cognitive Sciences*, *9*(12), 556–559. http://doi.org/10.1016/j.tics.2005.10.010

Massimini, M., Ferrarelli, F., Huber, R., Esser, S. K., Singh, H., & Tononi, G. (2005). Breakdown of cortical effective connectivity during sleep. *Science*, *309*(5744), 2228–2232. http://doi.org/10.1126/science.1117256

McLaren, D. G., Ries, M. L., Xu, G., & Johnson, S. C. (2012). A generalized form of context-dependent psychophysiological interactions (gPPI): a comparison to standard approaches. *NeuroImage*, *61*(4), 1277–1286. http://doi.org/10.1016/j.neuroimage.2012.03.068

Moeller, S., Yacoub, E., Olman, C. A., Auerbach, E., Strupp, J., Harel, N., & Ugurbil, K. (2010). Multiband multislice GE-EPI at 7 tesla, with 16-fold acceleration using partial parallel imaging with application to high spatial and temporal whole-brain fMRI. *Magnetic Resonance in Medicine*, *63*(5), 1144–1153. http://doi.org/10.1002/mrm.22361

Moore, C. I., Crosier, E., Greve, D. N., Savoy, R., Merzenich, M. M., & Dale, A. M. (2013). Neocortical correlates of vibrotactile detection in humans. *Journal of Cognitive Neuroscience*, *25*(1), 49–61. http://doi.org/10.1162/jocn_a_00315

Morey, R. D. (2008). Confidence Intervals from Normalized Data: A correction to Cousineau (2005). *Tutorial in Quantitative Methods for Psychology*, 61–64.

Naghavi, H. R., & Nyberg, L. (2005). Common fronto-parietal activity in attention, memory, and consciousness: Shared demands on integration? *Consciousness and Cognition*, *14*(2), 390–425. http://doi.org/10.1016/j.concog.2004.10.003

Newman, M. E. J. (2004). Analysis of weighted networks. *Physical Review E*, *70*(5 Pt 2), 056131. http://doi.org/10.1103/PhysRevE.70.056131

Odegaard, B., Knight, R. T., & Lau, H. (2017). Should a Few Null Findings Falsify Prefrontal Theories of Conscious Perception? *Journal of Neuroscience*, *37*(40), 9593–9602. http://doi.org/10.1523/JNEUROSCI.3217-16.2017

Oldfield, R. C. (1971). The assessment and analysis of handedness: the Edinburgh inventory. *Neuropsychologia*, *9*(1), 97–113. http://doi.org/10.1016/0028-3932(71)90067-4

Onnela, J.-P., Saramäki, J., Kertész, J., & Kaski, K. (2005). Intensity and coherence of motifs in weighted complex networks. *Physical Review E*, *71*(6 Pt 2), 065103. http://doi.org/10.1103/PhysRevE.71.065103

O'Reilly, J. X., Woolrich, M. W., Behrens, T. E. J., Smith, S. M., & Johansen-Berg, H. (2012). Tools of the trade: psychophysiological interactions and functional connectivity. *Social Cognitive and Affective Neuroscience*, *7*(5), 604–609. http://doi.org/10.1093/scan/nss055

Pleger, B., & Villringer, A. (2013). The human somatosensory system: From perception to decision making. *Progress in Neurobiology*, *103*, 76–97. http://doi.org/10.1016/j.pneurobio.2012.10.002

Power, J. D., Barnes, K. A., Snyder, A. Z., Schlaggar, B. L., & Petersen, S. E. (2012). Spurious but systematic correlations in functional connectivity MRI networks arise from subject motion. *NeuroImage*, *59*(3), 2142–2154. http://doi.org/10.1016/j.neuroimage.2011.10.018

Power, J. D., Cohen, A. L., Nelson, S. M., Wig, G. S., Barnes, K. A., Church, J. A., et al. (2011). Functional network organization of the human brain. *Neuron*, *72*(4), 665–678. http://doi.org/10.1016/j.neuron.2011.09.006

Preusser, S., Thiel, S. D., Rook, C., Roggenhofer, E., Kosatschek, A., Draganski, B., et al. (2015). The perception of touch and the ventral somatosensory pathway. *Brain*, *138*(3), 540–548. http://doi.org/10.1093/brain/awu370

Rees, G., Kreiman, G., & Koch, C. (2002). Neural correlates of consciousness in humans. *Nature Reviews Neuroscience*, *3*(4), 261–270. http://doi.org/10.1038/nrn783

Rorden, C., & Brett, M. (2000). Stereotaxic display of brain lesions. *Behavioural Neurology*, *12*(4), 191–200.

Rouder, J. N., Morey, R. D., Speckman, P. L., & Province, J. M. (2012). Default Bayes factors for ANOVA designs. *Journal of Mathematical Psychology*, *56*(5), 356–374. http://doi.org/10.1016/j.jmp.2012.08.001

Ruben, J., Schwiemann, J., Deuchert, M., Meyer, R., Krause, T., Curio, G., et al. (2001). Somatotopic organization of human secondary somatosensory cortex. *Cerebral Cortex*, *11*(5), 463–473.

Rubinov, M., & Sporns, O. (2010). Complex network measures of brain connectivity: uses and interpretations. *NeuroImage*, *52*(3), 1059–1069. http://doi.org/10.1016/j.neuroimage.2009.10.003

Sadaghiani, S., Poline, J.-B., Kleinschmidt, A., & D'Esposito, M. (2015). Ongoing dynamics in large-scale functional connectivity predict perception. *Proceedings of the National Academy of Sciences of the United States of America*, *112*(27), 8463–8468. http://doi.org/10.1073/pnas.1420687112

Schönbrodt, F. D., & Wagenmakers, E.-J. (2018). Bayes factor design analysis: Planning for compelling evidence. *Psychonomic Bulletin & Review*, *25*(1), 128–142. http://doi.org/10.3758/s13423-017-1230-y

Schröder, P., Schmidt, T. T., & Blankenburg, F. (2019). Neural basis of somatosensory target detection independent of uncertainty, relevance, and reports. *eLife*, *8*, 34. http://doi.org/10.7554/eLife.43410

Sperdin, H. F., Repnow, M., Herzog, M. H., & Landis, T. (2013). An LCD tachistoscope with submillisecond precision. *Behavior Research Methods*, *45*(4), 1347–1357. http://doi.org/10.3758/s13428-012-0311-0

Tononi, G. (2004). An information integration theory of consciousness. *BMC Neuroscience*, *5*, 42. http://doi.org/10.1186/1471-2202-5-42

Tononi, G., & Edelman, G. M. (1998). Consciousness and complexity. *Science*, *282*(5395), 1846–1851.

Tononi, G., Boly, M., Massimini, M., & Koch, C. (2016). Integrated information theory: from consciousness to its physical substrate. *Nature Reviews Neuroscience*, *17*(7), 450–461. http://doi.org/10.1038/nrn.2016.44

Uehara, T., Yamasaki, T., Okamoto, T., Koike, T., Kan, S., Miyauchi, S., et al. (2014). Efficiency of a “small-world” brain network depends on consciousness level: a resting-state FMRI study. *Cerebral Cortex*, *24*(6), 1529–1539. http://doi.org/10.1093/cercor/bht004

van Gaal, S., & Lamme, V. A. F. (2012). Unconscious high-level information processing: implication for neurobiological theories of consciousness. *The Neuroscientist*, *18*(3), 287–301. http://doi.org/10.1177/1073858411404079

Vatansever, D., Menon, D. K., Manktelow, A. E., Sahakian, B. J., & Stamatakis, E. A. (2015). Default Mode Dynamics for Global Functional Integration. *Journal of Neuroscience*, *35*(46), 15254–15262. http://doi.org/10.1523/JNEUROSCI.2135-15.2015

Weisz, N., Wühle, A., Monittola, G., Demarchi, G., Frey, J., Popov, T., & Braun, C. (2014). Prestimulus oscillatory power and connectivity patterns predispose conscious somatosensory perception. *Proceedings of the National Academy of Sciences of the United States of America*, *111*(4), E417–25. http://doi.org/10.1073/pnas.1317267111

Xia, M., Wang, J., & He, Y. (2013). BrainNet Viewer: a network visualization tool for human brain connectomics. *PLoS ONE*, *8*(7), e68910. http://doi.org/10.1371/journal.pone.0068910